Supporting Information for

Climate Models Underestimate Pre-Industrial Fire Emissions

Noah Liguori-Bills[1], Catherine E. Scott[2], Ken S. Carslaw[2], Natalie Kehrwald[3], Stijn Hantson[4], Susan Kaspari[5], Carlo Barbante[6], Elena Barbaro[6], Paolo Gabrielli[7,#], Roberta Zangrando[6], Lonnie G Thompson[8,9], and Douglas S. Hamilton[1]

[1]Marine, Earth, and Atmospheric Sciences, North Carolina State University, Raleigh, NC, USA.
[2]School of Earth, Environment and Sustainability, University of Leeds, Leeds, United Kingdom.
[3]US Geological Survey, Geosciences and Environmental Change Science Center, Denver, CO, USA.
[4]School of Sciences and Engineering, Universidad del Rosario, Bogotá, Colombia.
[5]Department of Geological Sciences, Central Washington University, Ellensburg, WA, USA.
[6]Ca'Foscari University of Venice, Mestre, Veneto, Italy
[7] Italian Glaciological Committee c/o University of Turin, Turin, Italy
[8]Byrd Polar and Climate Research Center, The Ohio State University, Columbus, OH, USA.
[9]School of Earth Sciences, The Ohio State University, Columbus, OH, USA.
[#]Now at the Metropolitan Water District of Southern California, 700 Moreno Ave, La Verne, CA, 91750, USA

Contents of this file

Additional Supporting Information (Files uploaded separately)

Table S9. Data within each ice core record.

Introduction

This document provides supporting information for the data analysis performed on modeled and ice core black carbon histories used in this study. Most analysis focused on the ratio of the present day (PD) and pre-industrial (PI) black carbon (BC) concentrations.

Text S1. Kilimanjaro Levoglucosan Ice Core Preprocessing

Levoglucosan is known to have very high temporal variability, in part because it reflects a more local burning regime than black carbon. Likewise, levoglucosan data was avoided in this analysis, however, the levoglucosan based Kilimanjaro ice core was included in the analysis because it was the only ice core record of burning on the entire African continent available to the authors.

Two levoglucosan values were given for the same timepoint in the ice core data: 4943 and 200 pg/mL levoglucosan at 1950 CE. Before any other preprocessing, these values were averaged into a single data point: 2571.5 pg/mL levoglucosan at 1950 CE. To reduce the temporal variability in the core's levoglucosan time series, lowess smoothing was used. To choose a lowess smoothing parameter, values between 0.25 and 0.5 on an interval of 0.05 were used to generate smoothed time series and the time series with the lowest parameter and without obvious issues was chosen. **Figure Kilimanjaro.1** showed each of these time series and their corresponding smoothing parameters. The only smoothing parameter that shows a clear issue is 0.3, which gives large negative values around -1000 CE. Therefore, the lowest viable smoothing parameter of 0.2 was chosen.

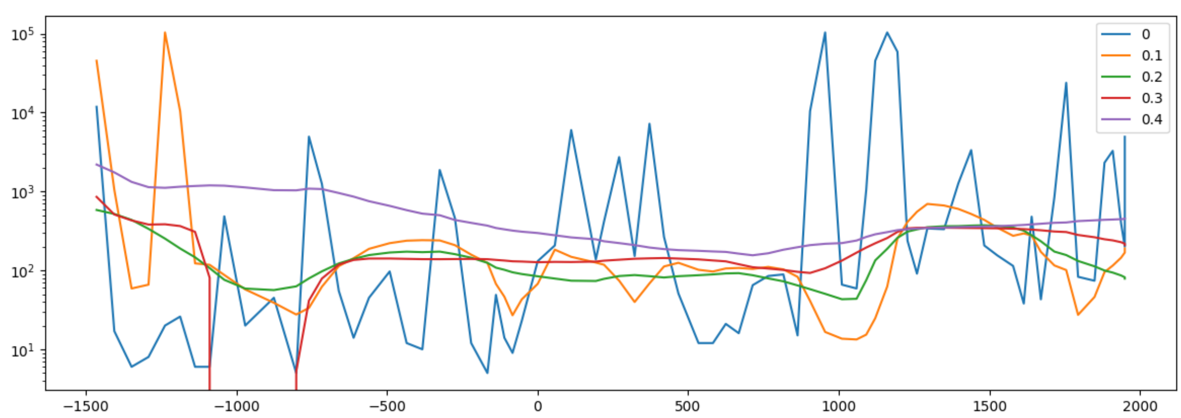

Figure S1. Kilimanjaro levoglucosan ice core (Core #9) logscale timeseries smoothed with different lowess smoothing parameters (0.1 to 0.4).

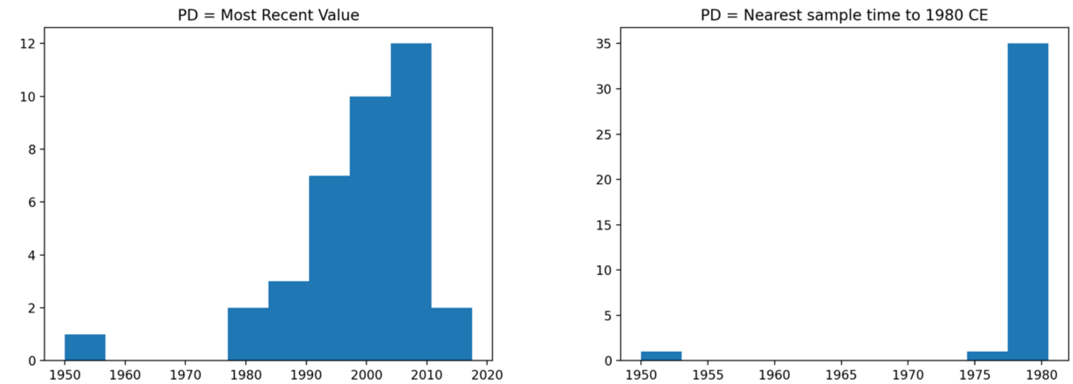

Figure S2. Histograms of each ice core's PD value using two different definitions: most recent value (left) and nearest sample date to 1980 CE (right). The PD year mean, standard deviation, and range were 1998.6, 12.3, and 67.5 for the most recent approach, and 1979.0, 4.92, and 30.5 for the 1980 approach respectively.

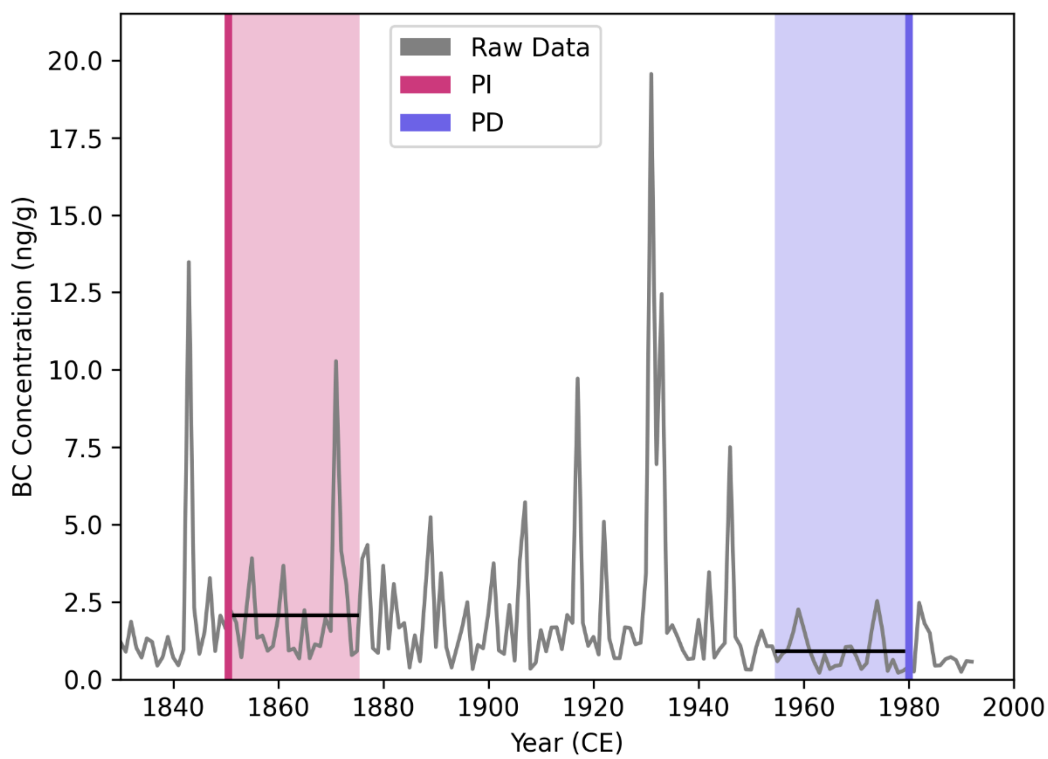

Figure S3. Example of methodology applied to each ice core. First the data with the nearest dates to 1850 and 1980 are found (thick pink and blue lines) then the 25 years of data shown in light pink and light blue are averaged to produce the BC values for PI and PD. Finally, these two numbers are divided to get the PD/PI ratio.

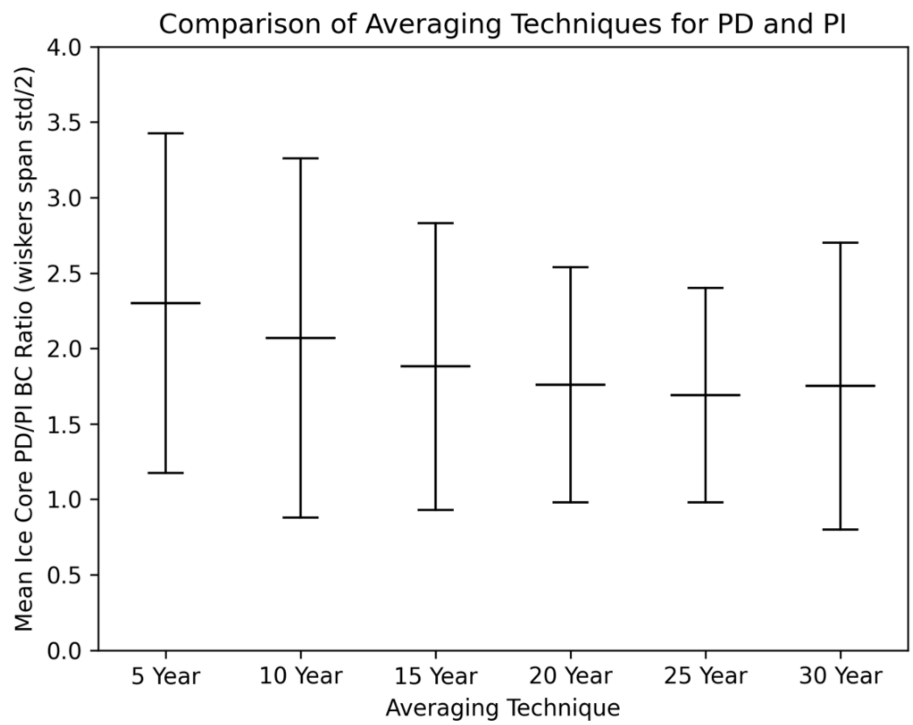

Figure S4. Comparison of averaging techniques for the ice cores' PD and PI.

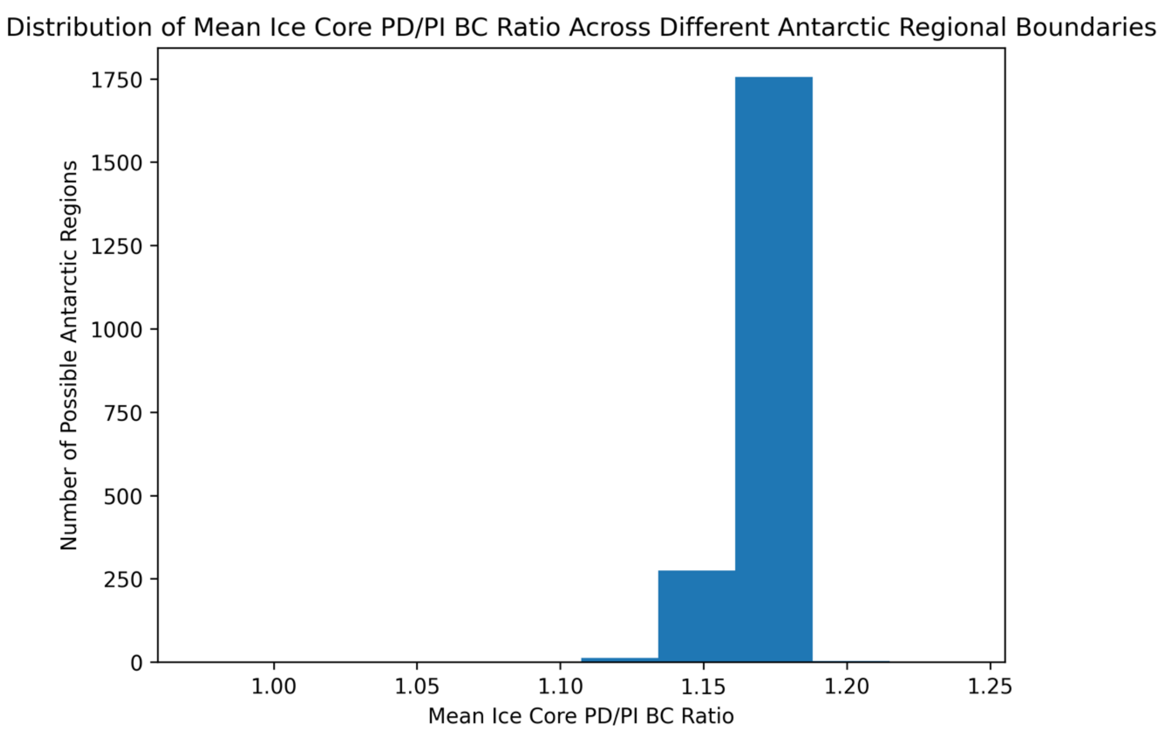

Figure S5. Histogram of every possible regional division of the Antarctic ice cores. All ice cores fall within a 0.1 PD/PI BC Ratio range.

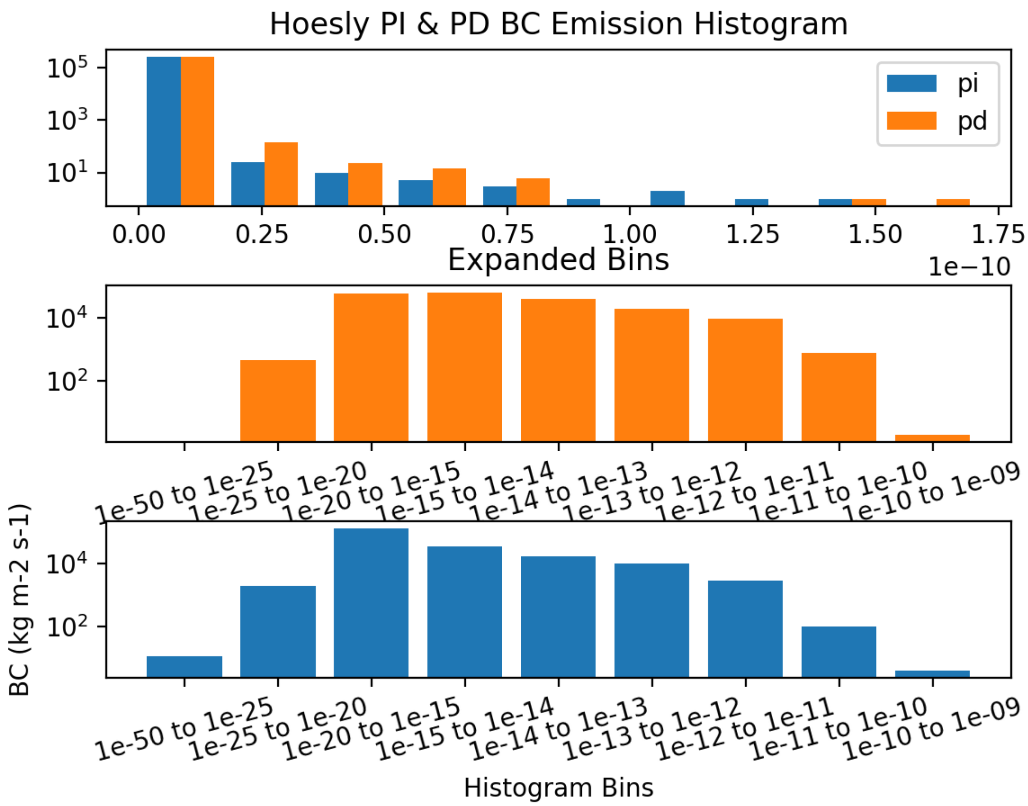

Figure S6. Histogram of global Hoesly anthropogenic BC emission sources in the PI and PD, highlighting low values less than 10^{-25} in the PI that skew PD/PI ratios high.

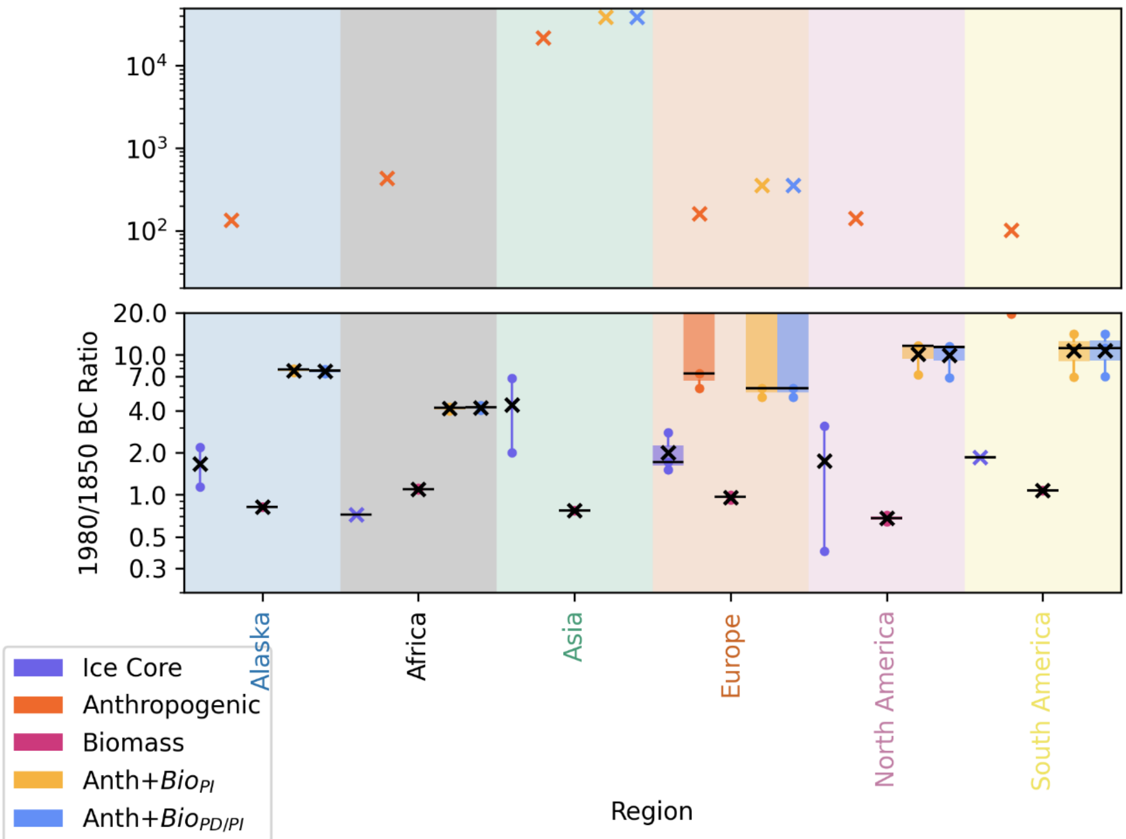

Figure S7. Using the emissions regions defined in section 2.3, results from Figure 3 were plotted against ice core values in Figure 4. These biomass PD/PI BC ratio means in each emission region (denoted with X's in Figure 3B) are relatively close to 1 (0.68 to 1.10), but are not within 40% of their corresponding ice core values in any region. Although 5/6 emission regions (Alaska, Asia, Europe, North America, and South America) showed mean Biomass ratios values below the ice cores', the Biomass BC dataset remains an overestimate because the combination Anthropogenic+Biomass PD/PI dataset, which best represents the total BC emissions that are captured by ice core records (as well as biomass, Anthropogenic+Biomass PI), all show regional ratio means above 400% of their corresponding ice core values, and frequently reach above 100, where the maximum ice core value in this dataset is 6.78.

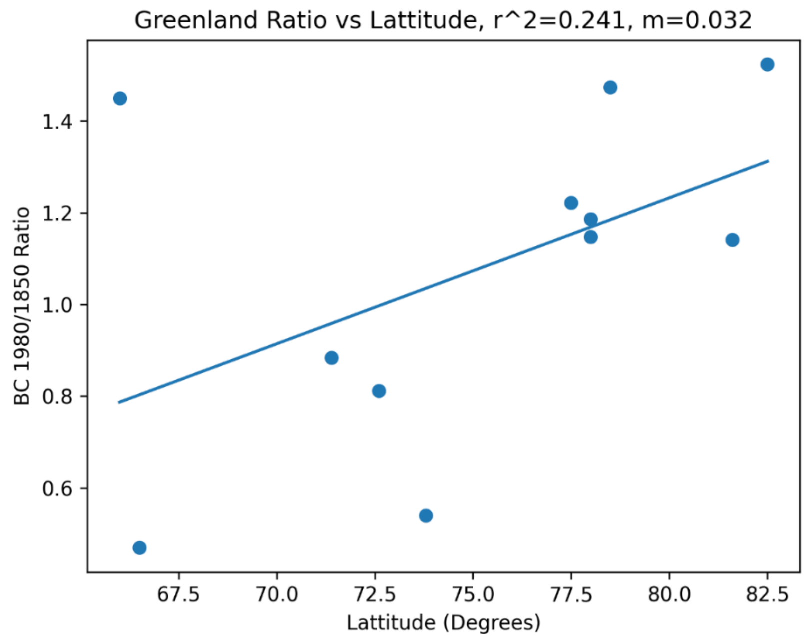

Figure S8. Correlation between Greenland ice cores' BC PD/PI ratio and latitude.

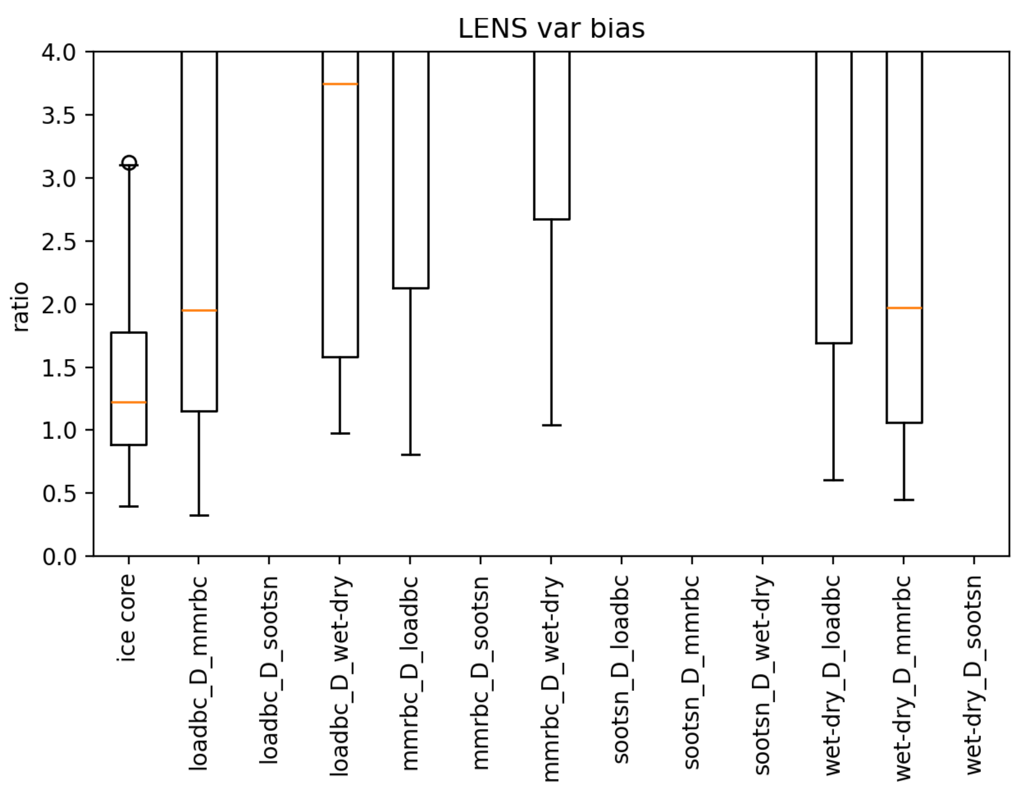

Figure S9. Comparison between various LENS variable biases (where var1 ÷ var2 is labeled as var1_D_var2) and the ice core. Bias labels with no data shown have an first quartile bound above 4.

Table S1. Overview of the existing BC ice core model evaluation literature and this work's contribution to the literature.

	This Study	**Hamilton et al., 2018**	**Liu et al., 2021**	**Moseid et al., 2022**	**Zhang et al., 2024**
Northern Hemisphere Ice Cores Used	24	4	0	15	16
Southern Hemisphere Ice Cores Used	13	0	14	1	15
Model BC Variables Used	Column Burden, Surface Conc., Deposition Flux, In Snow Conc	Surface Conc.	Surface Conc., Deposition Flux	Deposition Flux	Deposition Flux

Table S2. Comparison between different PI and PD averaging methods.

	5-year PD and PI	**10-year PD and PI**	**15-year PD and PI**	**20-year PD and PI**	**25-year PD and PI**	**30-year PD and PI**	**5-year PD and 25-year PI**
Mean ice core PD/PI BC ratio	2.30	2.07	1.88	1.76	1.69	1.75	2.10
Standard deviation in ice cores' PD/PI BC ratios	2.25	2.38	1.90	1.56	1.42	1.90	2.19
Minimum ice core PD/PI BC ratio	0.31	0.41	0.38	0.40	0.40	0.38	0.30
Maximum ice core PD/PI BC ratio	11.44	11.43	11.02	8.45	7.58	11.79	9.78

Table S3. Ice core data sources, latitude (degrees North) and longitude (degrees East), and common site abbreviations used.

Publication	Data Source	Latitude	Longitude	Site Abbrev-iation
Chellman et al. (2017)	https://doi.org/10.1021%2Facs.est.6b06574	43.1	-109.6	Upper Fremont Glacier
Zhang et al. (2024)	https://doi.org/10.18739/A2KH0F13W	66.5	-46.3	ACT11d
Zdanowicz et al. (2018)	https://www.polardata.ca/pdcsearch/PDCSearchDOI.jsp?doi_id=12952	75.32	-81.64	Devon Ice Cap
Zhang et al. (2024)	https://doi.org/10.18739/A2KH0F13W	73.8	-49.5	NasaU
Zhang et al. (2024)	https://doi.org/10.18739/A2KH0F13W	66	-45.2	ACT2
Zhang et al. (2024)	https://doi.org/10.18739/A2KH0F13W	72.6	-38.3	Summit2010
Zhang et al. (2024)	https://doi.org/10.18739/A2KH0F13W	69.3	-143.8	McCall Glacier
McConnell et al. (2007)	https://doi.org/10.25921/bphv-jy23	71.4	-44	D4
Thompson et al. (2002)	https://doi.org/10.1126/science.1073198	-3.076667	37.353333	NIF2
Zhang et al. (2024)	https://doi.org/10.18739/A2KH0F13W	78.5	-56.8	Humboldt
Zhang et al. (2024)	https://doi.org/10.18739/A2KH0F13W	77.5	-51.1	NEEM_2011_S1
Zhang et al. (2024)	https://doi.org/10.18739/A2KH0F13W	78	-33.8	Tunu2013
Liu et al. (2021)	https://doi.org/10.6084/m9.figshare.14251022	-66.769444	111.580833	W10
Zhang et al. (2024)	https://doi.org/10.18739/A2KH0F13W	82.5	-37.5	Hans Tausen
Liu et al. (2021)	https://doi.org/10.6084/m9.figshare.14251022	-78.6	35.6	NORUS_7_5
Arienzo et al. (2017)	https://doi.org/10.15784/601034	-75	0.1	B40
Taylor et al. (2011)	https://doi.org/10.15784/600142	-79.4676	-112.0865	WAIS DIVIDE
McConnell et al. (2022)	https://doi.org/10.18739/A2W37KX21	81.6	-15.7	Flade Isblink
McConnell et al. (2021)	https://doi.org/10.15784/601464	-76.8	31.9	B53
Sigl et al. (2018)	https://doi.org/10.1594/PANGAEA.894788	45.932	7.876	CG15

Zhang et al. (2024)	https://doi.org/10.18739/A2KH0F13W	78	-36.4	NGT_B19
Liu et al. (2021)	https://doi.org/10.6084/m9.figshare.14251022	-73.5833	-70.3667	Gomez
McConnell et al. (2021)	https://doi.org/10.15784/601464	-82.1	54.9	NORUS_7_7
McConnell et al. (2021)	https://doi.org/10.15784/601464	-74.1	1.6	NUS08_7
Ruppel et al. (2014)	https://doi.org/10.23728/fmi-b2share.858bbae80cde4b26bda0a37a56d7db99	79.1375	13.272222	Holtedahl-fonna Glacier
Osmont et al. (2019)	https://doi.org/10.25921/3ygy-q259	-16.65	-67.7833	Illimani Glacier
Legrand et al. (2024)	https://www.ncei.noaa.gov/access/paleo-search/study/38580	43.3483	42.4267	Mount Elbrus
Osmont et al. (2018)	https://doi.org/10.25921/gqct-0c60	78.8234	17.4331	LF-09
Zhang et al. (2024)	https://doi.org/10.18739/A2KH0F13W	60.5	-139.5	Eclipse
Matthew et al. (2016)	https://doi.org/10.1016/j.accre.2016.07.002	33.576667	91.179333	Guoqu Glacier
McConnell et al. (2021)	https://doi.org/10.15784/601464	-64.2	-57.7	JRI_2008
Liu et al. (2021)	https://doi.org/10.6084/m9.figshare.14251022	-71.167	111.367	Aurora Basin
Zhang et al. (2024)	https://doi.org/10.18739/A2KH0F13W	80.5	94.8	Akademii Nauk
Liu et al. (2021)	https://doi.org/10.6084/m9.figshare.14251022	-76.1	22.5	NORUS_7_2
Kaspari et al. (2020)	https://doi.org/10.1029/2019JD031126	48.3564	-121.0574	SCG
Eichler et al. (2023)	https://www.ncei.noaa.gov/metadata/geoportal/rest/metadata/item/noaa-icecore-37972/html	46.551	8.067	FH
Barker et al. (2021)	https://doi.org/10.25921/vxax-w749	28.3833	85.7167	Dasuopu Glacier

Table S4. Region definitions and number of ice cores in each region.

Large Region	Region	Definition	Number of Ice Cores
North Pole	Arctic	All areas above 66.6 degrees North in latitude except Greenland	5
	North Greenland	Greenland's land area above 71.5 degrees North in latitude	8
	South Greenland	Greenland's land area below 71.5 degrees North in latitude	3
South Pole	Antarctic	Continental Antarctica	11
Alpine	Africa	Continental Africa	1
	Asia	Continental Asia	2
	Europe	Continental Europe, Eastern Europe and the Middle East	3
	North America	All areas in continental North America below 67 degrees North in latitude	3
	South America	Continental South America	1

Table S5. The ensemble, subset, and comparisons of each model used in this analysis.

Ensemble	Ensemble Subset	Model	Deposition Comparison	3 Variable Comparison
LENS1	Members 18-35	CESM1	X	
CMIP6	CESM2	CESM2	X	X
		CanESM5	X	
		CESM2_re	X	
		MIROC	X	
		EC-Earth	X	
		MRI	X	
		CNRM	X	
		IPSL	X	

Table S6. The max, min, and mean absolute and standard deviation differences between different grid box averaging methods for LENS data. S4 and S8 represent averaging the 4 and 8 nearest grid boxes to an ice core's latitude and longitude, respectively, and S1 represents using the raw data from the nearest grid box without any grid box averaging.

	Max	**Min**	**Mean**
S4 - S1	2.43	-1.78	-0.1
S8 - S1	3.15	-2.61	-0.16
std(S4) - std(S1)	0.97	-5.61	-0.56
std(S8) - std(S1)	2.22	-7.75	-0.67

Table S7. The absolute and standard deviation differences between different vertical level averaging methods for LENS data. LV30 and LV28 represent the nearest and the third nearest model levels to the Earth's surface, respectively.

	Max	**Min**	**Mean**
LV30 - LV28	8.60×10^{-3}	7.04×10^{-8}	2.59×10^{-4}
std(LV30) - std(LV28)	2.15×10^{-3}	5.33×10^{-7}	2.67×10^{-4}

Table S8. Regional PD/PI BC medians for each CESM2 model variable explored in Figure 6.

Regions	**Ice Core**	**BC in air column**	**BC deposition to snow**	**BC in surface air**	**BC in snow**
North Pole	1.17	3.02	3.86	2.64	1.98
South Pole	1.05	3.14	3.26	2.59	1.91
Alpine	1.93	3.69	2.75	2.67	3.90